J Biomed. Eng. Res.
Vol. 21, No. 4, 391-101, 2000

벽-유체의 상호작용을 고려한 유연관 내부 유동의 수치적 연구

심 은 보

금오공과대학교 기계공학부

(2000년 3월 4일 접수, 2000년 8월 10일 채택)

Numerical Analysis of the Flow in a Compliant Tube Considering Fluid-wall Interaction

E.B. Shim

Department of Mechanical Engineering Kumoh National University of Technology

(Received March 4, 2000. Accepted August 10, 2000)

요 약 본 연구에서는 정맥 등과 같은 혈관의 상황을 모사하기 위하여 선형적으로 벽 두께가 변하는 축 대칭 관의 벽면과 유체 유동의 상호작용을 유한요소 방법으로 해석하였다. 사용한 유한요소 상용 소프트웨어(ADINA)의 타당성을 검증하기 위해서 막힘이 있는 혈관에서의 벽과 혈류의 상호작용을 해석하고 이를 기존의 실험결과와 비교하였다. 또한 2차원 신축 벽을 가지는 평판 사이의 유체 유동에 대한 결과를 기존 연구결과와 비교하였다. 축대칭 문제의 경우, 입구의 압력은 일정하게 유지하면서 출구 압력을 감소시켜 나간다. 출구 압력의 감소에 따라, 유량은 증가하며, 관내 유로의 단면적은 감소한다. speed index(평균속도를 파의 속도로 나눈 값)가 1 근방에서 유량은 최대가 되며, 유로 단면적이 최소가 된다. 그리고 출구압력이 좀 더 감소하면 유량은 오히려 줄어든다. 이와 같은 현상을 유동제한(flow limitation) 혹은 초킹(choking)이라 하는데, 폐의 기도(airway) 및 모세혈관, 그리고 이외의 여러 정맥들에서 자주 발생하는 폭포효과의 원인이 된다. 상류벽 두께와 하류 벽두께의 비가 2일 경우에는 하류 쪽에서 목(area throat)이 형성되며 이 비가 3일 경우에는 상류 쪽으로 이동하는데 이는 하류 벽면의 강성(stiffness)이 상류 쪽에 비해 강하게 되어서 상류 쪽에서 먼저 붕괴가 일어나기 때문이다.

Abstract : Flow through compliant tubes with linear taper in wall thickness is numerically simulated by finite element analysis. For verification of the numerical method, flow through a compliant stenotic vessel is simulated and the results are compared to the existing experimental data. Steady two-dimensional flow in a collapsible channel with initial tension is also simulated and the results are compared with numerical solutions from the literature. Computational results show that as cross-sectional area decreases with the reduction in downstream pressure, flow rate increases and reaches the maximum when the speed index (mean velocity divided by wave speed) is near the unity at the point of minimum cross-section area, indicating the flow limitation or choking (flow speed equals wave speed) in one-dimensional studies. For further reductions in downstream pressure, flow rate decreases. The flow limitation or choking consist of the main reasons of waterfall effect which occurs in the airways, capillaries of lung, and other veins. Cross-sectional narrowing is significant but localized. When the ratio of downstream-to-upstream wall thickness is 2, the area throat is located near the downstream end. As this ratio is increased to 3, the constriction moves to the upstream end of the tube.

Key words 붕괴 가능한 관(collapsible tube), 유체-고체 상호작용(fluid structure interaction), 막힘이 있는 혈관(stenotic vessels), 유동 제한(flow limitation), 유한요소 상용코드 ADINA(finite element commercial package ADINA)

Introduction

In many practical situations the fluid dynamic forces acting on a physiologic vessel cause the walls to undergo significant deformation. These deformations frequently influence the rate of flow through the vessel and can also elicit important biological effects. Examples in the first category include collapse of the veins above the level of

이 논문은 한국과학재단의 해외 Post-doc 연수지원비에 의하여 연구되었으며 이에 감사드립니다.

통신지자 심은보, (730-701) 경북 구미시 신평동 188 금오공과대학교 기계공학부
Tel (054)467-4207, Fax (054)467-4050
E-mail. simeb@knut.kumoh.ac.kr

the heart, flow limitation during a forced expiration, and the waterfall effect in the pulmonary microvascular bed[1]. Other, biological effects arise from the deformation of the vessel wall, resulting in altered gene expression or secretion of various agents, such as, cytokines or growth factors.

Numerous studies have been conducted on vessel collapse using experimental or numerical methods. Experiments by Conrad[2], Brower et al.[3], and Bertram[4], have demonstrated the rich variety and complexity associated with such phenomena as flow limitation and self-excited oscillations. Numerical investigations based on the assumption of one-dimensional flow have reproduced many of these same phenomena. This simple approach worked remarkably well in the prediction of flow limitation[5, 6] and large amplitude flow induced oscillations[7]. Questions still remained however, concerning the precise physical mechanism of flow instability in certain types of flutter. Because of the simplifying assumptions on which the analyses were based, they were obviously not capable of addressing issues involving two- or three-dimensional effects.

In order to produce a more realistic simulation, Pedley[8] first examined steady, two-dimensional flow in a collapsible channel at low Reynolds number using lubrication theory. Extending this work, Luo & Pedley[9, 10] solved the full Naiver-Stokes equations for steady and unsteady flow, again for a two-dimensional collapsible channel. In these studies, the wall was modeled as an elastic membrane having zero thickness. This is a useful simplification for thin-walled vessels but one which fails to account for bending stiffness and in-wall shear stresses that are important in a wall of finite thickness. This assumption provides no information on the stress distribution inside the vessel wall. More recently, Heil[11] produced a three-dimensional solution of flow through a collapsible tube using a Stokes flow approximation for the fluid and a shell model for the wall, respectively. His results accurately reproduce the three-dimensional character of vessel collapse and compare favorably with experiments but have thus far been restricted to low Reynolds number flow and thin-walled vessels.

Using a finite element code that solves the fully nonlinear equations for the solid and fluid, Bathe & Kamm[12] recently analyzed flow at high Reynolds number through an axisymmetric stenotic vessel. Though the axisymmetric assumption precluded buckling of the wall, the solutions allowed for significant inertial effects in the fluid and provided detailed information on the stress field within the elastic wall. The deformations computed in that work, however, were relatively small due to the stiffness of the arterial wall and stenosis relative to the magnitude of pressure fluctuations.

In this study we use the same approach as Bathe & Kamm[12], but consider a problem with large amplitude wall deformations. Axisymmetric flow is considered under conditions that lead to flow limitation. In an attempt to minimize the influence of the downstream rigid attachment point, models of tubes are used that have a linear taper in wall thickness. Flow is induced by a progressive reduction in downstream pressure. Steady solutions for given pressure differences are obtained solving the full Navier-Stokes equations and the equilibrium equations for the solid elastic wall having finite thickness. We examine varying degrees of wall taper to elucidate its effect on vessel collapse. A commercial finite element package ADINA[13] is employed to accurately simulate the essential character of fluid structure interactions. To validate the accuracy of the code, we solve for flow and deformation in a stenotic compliant tube and two-dimensional collapsible channel, and compare the numerical predictions to existing experimental and numerical data.

Computational Model and Methods

Flow through flexible-walled vessels is simulated using the commercial package ADINA[13]. Response of the elastic wall is analyzed using the standard Lagrangian formulation for which the governing field equations evaluated at each time step in the analysis are

$$\tau_{ij,i} = \rho_s \ddot{u}_i \tag{1}$$

where ij is the ij-th component of the Cauchy stress tensor (i,j = 1,2), $\ddot{u}_i$ is the material particle acceleration in the coordinate i direction, and ρ_s is the density of solid. The comma denotes partial differentiation. ADINA uses a mixed displacement/pressure-based finite element formulation to solve these equations. In the solutions presented here, nine-node axisymmetric quadrilateral elements with quadratic displacement interpolation and linear element pressure are employed.

The governing equations for viscous incompressible fluid flow are obtained from the principles of mass and momentum conservation. The equations in vector notation are

$$\frac{\partial U}{\partial t} + \nabla \cdot (F - G) = 0 \tag{2}$$

where

$$U=\begin{bmatrix} 0 \\ \rho_f \vec{v} \end{bmatrix}, \quad F=\begin{bmatrix} \rho_f \vec{v} \\ \rho_f \vec{v}\,\vec{v} \end{bmatrix}, \quad G \begin{bmatrix} 0 \\ \tau \end{bmatrix} \tag{3}$$

and where $\vec{v}$ is the velocity vector; ρ_f is fluid density, and τ is the stress tensor, the components of which are given by

$$\tau_{ij} = -p\delta_{ij} + 2\mu e_{ij} \tag{4}$$

Here p is fluid pressure, δ_{ij} the Kronecker delta, μ the coefficient of viscosity, and the components of the strain rate tensor are given by

$$e_{ij} = \frac{v_{i,j} + v_{j,i}}{2} \tag{5}$$

Application of the usual Galerkin finite element discretization for equation (2) yields the following matrix equations in symbolic form:

$$KX = R \tag{6}$$

where K is the stiffness matrix, X is the vector of unknown nodal variables (velocities and pressure) and R contains the external driving forces. Three-node axisymmetric triangular elements with a linear interpolation function for velocity and pressure and an additional bubble velocity function are used to discretize the fluid domain in equation (2). Since the matrix equation above, derived from fluid governing equation (2), is highly nonlinear it must be solved by an incremental iterative scheme such as the Newton-Raphson method or the method of successive substitution within each time step[13]. A similar matrix equation for the solid is derived from application of the variational principle to equation (1) and discretization of the solid solution domain with nine-node axisymmetric quadrilateral elements having a quadratic displacement interpolation function. In the solid matrix equation, the unknown variables are the nodal displacement vectors.

To simulate interactions between the fluid and solid domains, ADINA utilizes the Arbitrary Lagrangian Eulerian (ALE) formulation[13] requiring that the momentum equation in (2) be modified to account for mesh movement. This necessitates a simple change in the convective term leading to the form given below:

$$\rho\left[\frac{\delta v_i}{\delta t} + \left(v_j - \frac{\delta d_j}{\delta t}\right) v_{i,j}\right] = \tau_{ij,j} \tag{7}$$

where $\frac{\delta v_i}{\delta t}$ is the time-derivative of the velocity component v_i at the position of the moving mesh point considered, and $\frac{\delta d_j}{\delta t}$ is the velocity of the moving mesh in the j-th direction.

Solution of the fluid and solid equations is accomplished by a fully-coupled method satisfying force equilibrium and matching of the velocities and displacements at each nodal point for each time step during the computation. This is accomplished by an iterative technique between the fluid and solid solvers until attaining the desired convergence.

Results and Discussion

1. Verification of the code

ADINA was developed originally for the solution of structural problems, and extended in recent years to add the capability for solving fluid flow or fluid-structure interaction(FSI) problems. Since then, it has been used for a variety of fluid-structure interaction problems in engineering, many of which can be found in the literature[12, 13, 14]. Here we present two validation studies in which the vessel compliance is a dominant factor.

1) Flow through a compliant tube with a localized constriction

In order to test the FSI capabilities of the code, we solve for steady flow through a stenotic compliant tube and compare our results with existing experimental data[15]. For this computation the working fluid is water and the membrane is made of rubber, modeled here using the Mooney-Rivlin description. The ratio of bulk modulus to shear modulus is set equal to 1500, giving a Poisson ratio of 0.4997 in this linear elastic analysis. The geometry of the stenotic tube is shown in Fig. 1(a), selected to mimic that used in the Stergiopulos experiments. As seen in the figure, the stenosis extends for a length of Ls=30mm and has an unobstructed diameter D0 of 8mm. The stenosis diameter at zero transmural

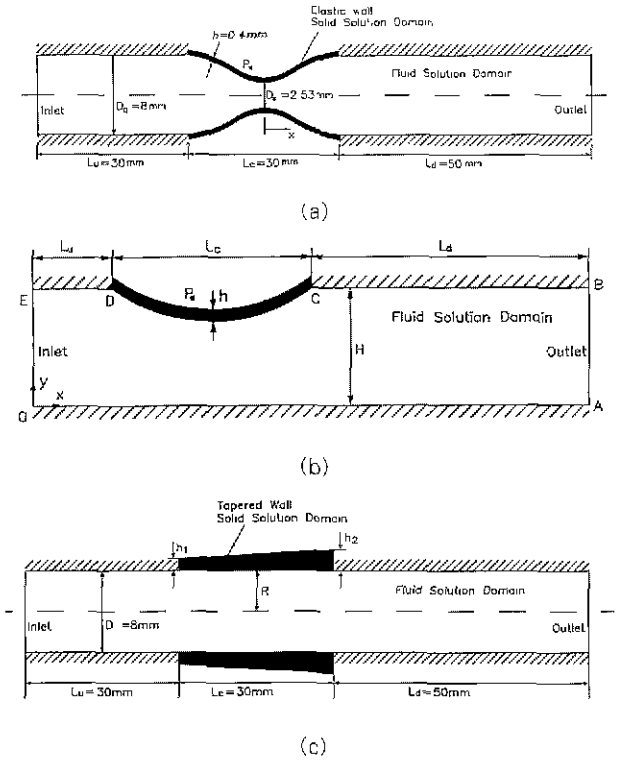

Fig. 1. Tube and channel geometries from the present simulations: (a) The stenotic tube with elastic wall as used in the study by Stergiopulos et al [15] (b) The two-dimensional collapsible channel with initial tension as used by Luo & Pedley [9] (c) An axisymmetric compliant tube

pressure Ds is 2.53 mm so that the severity of the stenosis defined as $[1-D_s^2/D_0^2]\times 100 = 90\%$. We use the following equation for the shape of the stenosis as in the case of Stergiopulos's experiment.

$$D(x) = D_0 - \frac{D_0 - D_s}{2}\left[1-\cos\left(\frac{2\pi x}{L_c}+\pi\right)\right] \qquad (8)$$

The mesh system of the fluid region is composed of 4,848 triangular elements and 2,639 nodes and 122 elements and 315 nodes in solid domain. During the simulation, inlet pressure is held constant at a value of Pin=74mmHg and outlet pressure Pout is decreased from 74mmHg in 1mmHg increments External pressure Pe is maintained constant at 3mmHg. At each pressure, the simulation is continued until the solution becomes steady This procedure is followed until Pout = 41mmHg, at which point the numerical solution is no longer able to converge Since at this stage the Reynolds number based on average outlet velocity and unobstructed diameter is 2478, solutions for lower downstream pressures would be strongly influenced by turbulence, the effects of which are absent from our analysis. In addition, as discussed below, the transmural pressure is beyond that needed to buckle the tube, thus invalidating the assumption of axisymmetry. Thus, while the cause of the solution breakdown is unknown, there is good reason based on physical grounds, not to attempt to continue the solution any further since the results would be increasingly unrealistic

The streamlines obtained from this solution exhibit a large region of recirculating flow downstream of the stenosis, as one would expect in the vicinity of a sudden expansion Pressure attains a minimum value at the throat, raising the possibility of collapse of the stenotic tube at that point. Progressing downstream from the stenosis, the pressure increases, corresponding to flow deceleration with some pressure recovery. Figs. 2(a) & (b) show the variations of flow rate and internal diameter of the stenosis as functions of outlet pressure. When the pressure difference is small, there is good agreement between the measured and predicted flow rates and internal diameter of the stenosis. As the pressure difference increases, however, the numerical solutions deviate some from the experimental values due to the three dimensional effects as pointed out by Stergiopulos et al [15]. The computations are terminated at a pressure difference of 41mmHg prior to the point where the experimental results show flow limitation and tube collapse. For the reasons mentioned above, and because of the reported tendency for flow-induced oscillation at higher flow rates, no attempt was made to continue the calculations any further.

2) Steady flow through a two-dimensional collapsible channel

The results of Luo & Pedley[9] are chosen for

Table 1. Parameters used by Luo & Pedley (1995) for simulation of flow through a two-dimensional channel with a thin membrane

Fluid density:	103kg/m^3
Fluid viscosity	10-3kg/(ms)
Reference initial tension: T_0	1.61 N/m
External pressure P_e	0.93 Pa
Channel height: H	0.01 m
Collapsible length: L	0.05 m
Downstream length: L_d	0.07 m
Upstream length: L_u	0.02 m

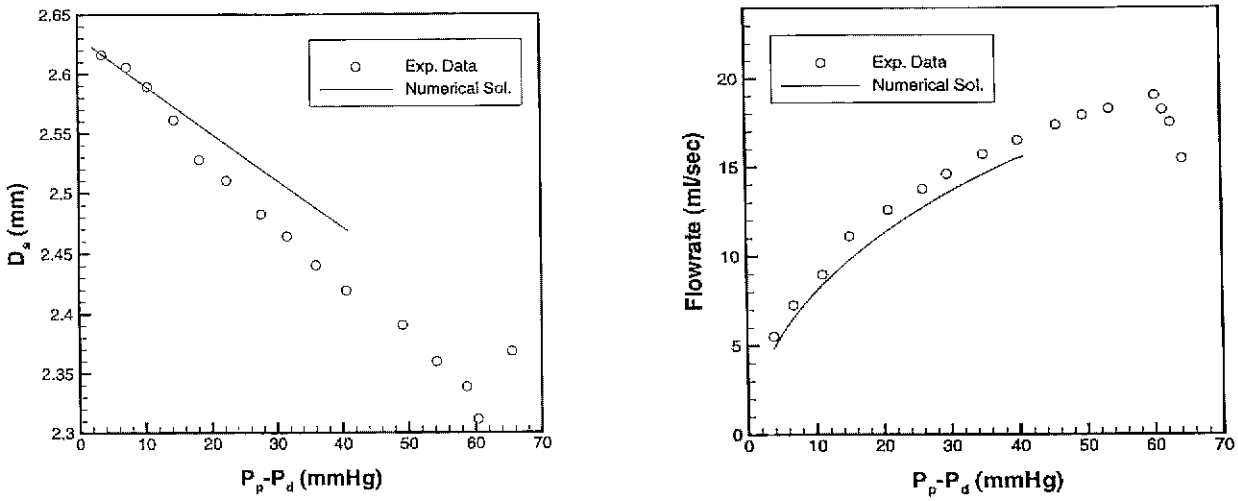

Fig. 2. Comparisons of computed results to experimental data by Stergiopulos, et al.[15]. (a) Stenotic diameter versus pressure difference. (b) Flow rate versus pressure difference

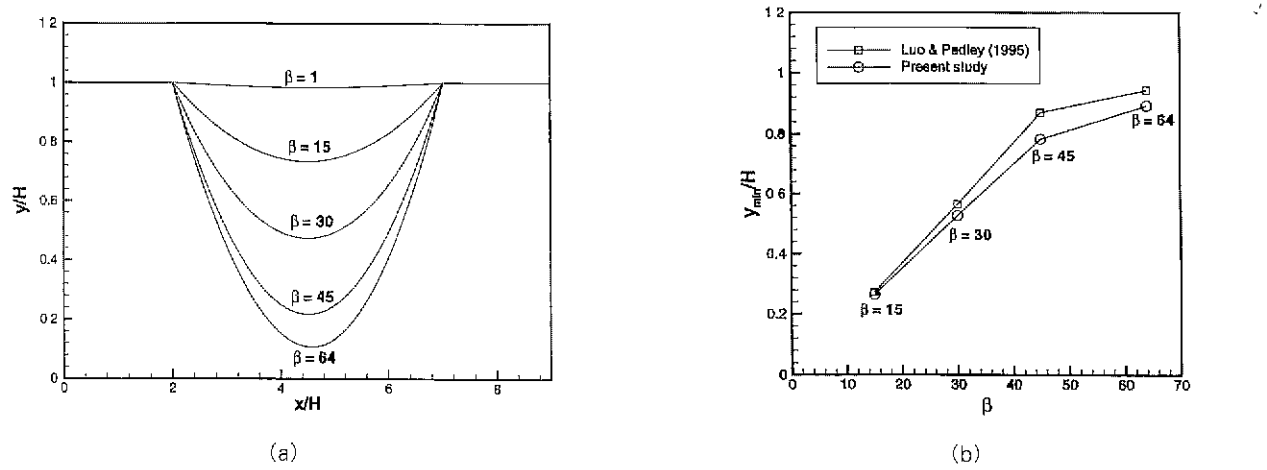

Fig. 3. (a) Deformed shapes of the collapsible wall according to several values of β(=T/T_0 where T_0=1.61N/m). (b) Comparisons of the computed maximum displacement versus β to the results of Luo & Pedley[9]. The minimum channel height is Y_{min}

comparison with the steady two-dimensional fluid-structure interaction simulation. Luo & Pedley used the full Navier-Stokes equations to analyze the fluid flow but employed a thin membrane approximation with non-zero initial tension in the compliant wall. The detailed geometry of the problem is depicted in Fig. 1(b) and the parameter values used in Luo & Pedley are presented in Table 1. In every instance, we specified the same parameter values used by Luo & Pedley. Additional parameters were required for the solid wall in our simulation due to its finite thickness. In collapsible tube problems, it has been shown that the computation based on the solid wall with thin thickness can produce some similar result with the calculation using the assumption of thin membrane[11] To produce a situation that most closely approximates that of a thin membrane in constant tension, we set the Young's modulus of the linear elastic solid(E) to 10 Pa, the Poisson ratio to 0.0 and the wall thickness to 10% of the channel height H. No-slip boundary conditions were imposed at the wall segments OA, ED, and CB; a parabolic velocity profile was assumed at the entrance EO with zero normal traction at the outflow boundary AB. We calculated the solution for Re=1 where Reynolds number is based on channel height and the

Table 2 Material properties and reference values used in simulations of an axisymmetric compliant tube

Fluid density : ρ	103kg/m^3
Fluid viscosity : μ	10-3kg/(ms)
Elastic modulus of solid : E	2×103N/m^2
Poisson ratio of solid : ν	0 3
Unobstructed area : $A_0=\pi R^2$	5×10-4 m^2
Reference pressure : $P_{ref}=Eh_1/R$	200 Pa
Reference flow rate : $Q_{ref}=\pi R^2(Eh_1/\rho D_0)^{1/2}$	15 8 ml/s

mean velocity at the entrance of the channel for the purpose of comparison to published results

Luo & Pedley imposed an initial tension in the wall, specified as $T=T_0/\beta$ where T0 is a constant tension and β is a scaling factor. Higher β implies lower initial tension in the wall and consequently greater deformation for the same transmural pressure difference. Fig. 3 shows deformed shapes for several values of β and Fig 4 indicates the maximum deformation As can be seen in Fig. 4, while the agreement with Luo & Pedley (Fig. 4(a) in their paper) is generally good, the maximum displacement of the wall in the present study is somewhat differentfrom the value previously reported. This is because Luo & Pedley assumed constant tension during the deflection process whereas the wall tension will naturally increase in our simulation as deformation increases. For example, the tension in the deformed state is larger than the initial tension by 8% for β=64, accounting for the deviations of maximum displacement between our computation and that of Luo & Pedley

2. Axisymmetric tube with tapered wall

The axisymmetric model used in the this simulation is shown in Fig. 1(c). Here, h1, the upstream wall thickness, is held constant at 0.4mm. Wall thickness tapers linearly to a minimum value, h_2, at the downstream end. The tube length-to-radius ratio, Lc/R, is equal to 7.5 and tapers h_2/h_1 of 1, 2, 3, and 4 are used The tube wall is taken to be linearly elastic with Young's modulus of 2×10^3 Pa All other parameter values are given in Table 2. The reference pressure is proportional to the ratio (h1/R) and Young's modulus E and the reference flow rate is defined using the wave speed in Eq (9) and the cross sectional area πR^2

Table 3 Maximum Reynolds number at each wall thickness ratio in axisymmetric tube simulation

h_2/h_1=1	$(Re)_{max}$=910 3
h_2/h_1=2	$(Re)_{max}$=1141.4
h_2/h_1=3	$(Re)_{max}$=1238.8
h_2/h_1=4	$(Re)_{max}$=1285.9

A no slip wall boundary condition is applied in the fluid along lines AB and CD while symmetry is assumed around line EF. Line BC coincides with line IJ of the solid domain constituting the fluid-structure interaction boundary (Fig 1). It is along this boundary that displacements and traction forces are passed between the fluid and solid domains In these simulations, the fluid and solid domains are discretized as shown in Fig. 4. The mesh consists of 3,383 nodes, 6,227 triangular elements clustered in both ends of the elastic wall for the fluid domain and 140 quadrilateral elements for the solid domain. To assess mesh dependency, computational results using finer (one third more mesh points) and coarser(one third fewer) mesh points for h_2/h_1=1 produced differences in flow rate and minimum area reduction of less than 2.5%.

Flow is induced by the pressure difference $\Delta P=P_{in}-$

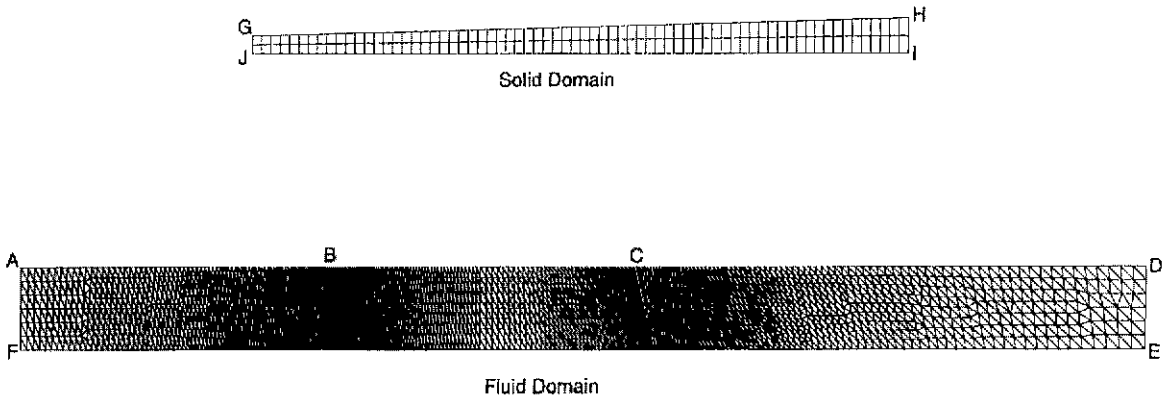

Fig. 4. Mesh system for the axisymmetric tube with 6 227 triangular fluid elements and 140 quadrilateral solid elements

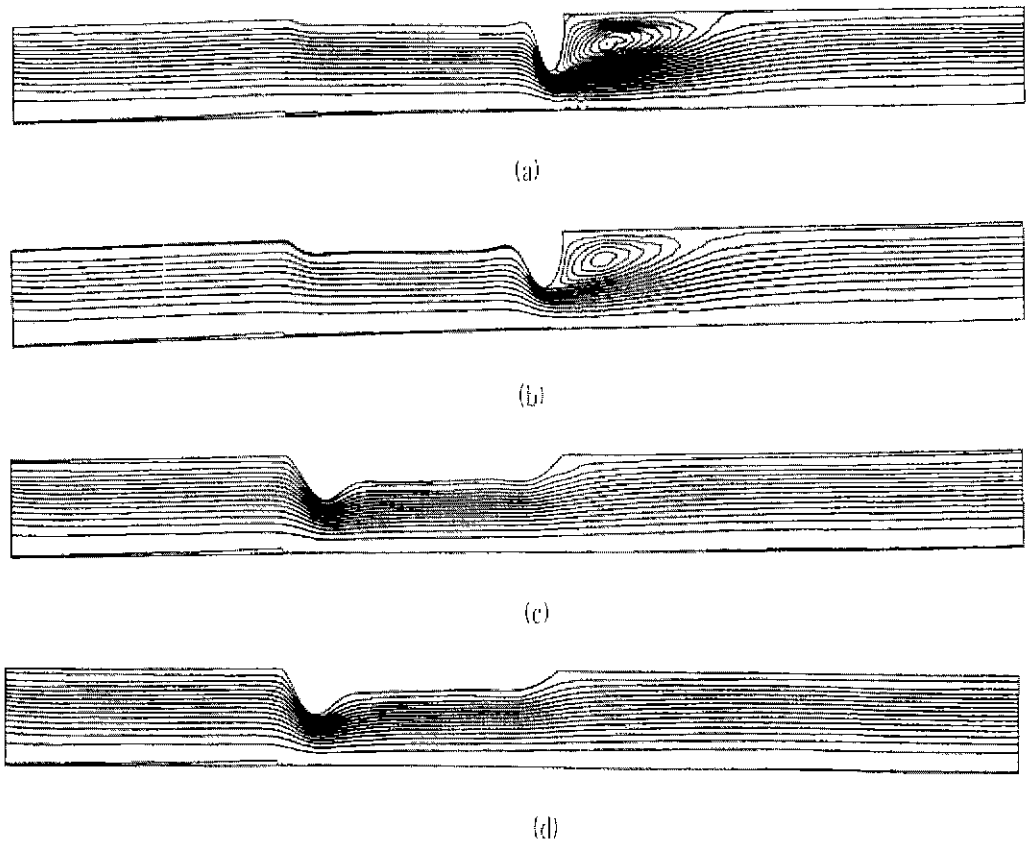

Fig. 5. Streamline patters in the axisymmetric tybe corresponding to the maximum pressure difference before loss of convergence (a) $h_2/h_1=1$ at $\Delta P/P_{ref}=0.6$, (b) $h_2/h_1=2$ at $\Delta P/P_{ref}=1.4$, (c) h2/h1=3 at $\Delta P/Pref=0.6$ (d) $h_2/h_1=4$ at $\Delta P/P_{ref}=0.6$

Pout between inlet and outlet. Inlet pressure and external pressure are maintained constant at Pin= Pe=0 while downstream pressure is decreased in 5 Pa increments, allowing the solution to converge at each condition. The computations are conducted in a step-wise manner using the steady solution from the previous step as the initial guess for the next calculation.

Maximum Reynolds numbers at each wall thickness ratio are given in Table 3 where it is seen that the largest value, 1200, occurs in the tube with the largest mean wall thickness ($h_2/h_1=4$). Streamlines at the condition of maximal pressure difference just prior to loss to convergence are plotted in Fig. 5 for the four values of wall thickness ratio. Narrowing is highly localized near downstream end of when the tube is of uniform thickness ($h_2/h_1=1$) or when the taper is mild ($h_2/h_1=2$). Regions of recirculating flow are observed for these two cases due to the high degree of narrowing and the relatively abrupt area increase downstream of the minimum area point Figure 6 shows flow rate increasing as downstream pressure is reduced, rapidly at first, then slowing, reaching a maximum, and finally falling gradually as the tube becomes increasingly collapsed. This pattern is suggestive of wave speed flow limitation as is often observed in collapsible tube flow[6], although the drop in flow rate after reaching the peak is not predicted by the previous one-dimensional theories. This behavior is discussed more fully below.

When the degree of wall taper is large ($h_2/h_1=3$ or 4), the behavior is distinctly different. The point of minimum area moves to a location near the upstream end of the tube, and the recirculation zone is less pronounced or completely absent due to the more gradual area increase downstream. Variations in minimum area are particularly interesting showing, in contrast to cases with milder taper, an increasingly steep drop as downstream pressure

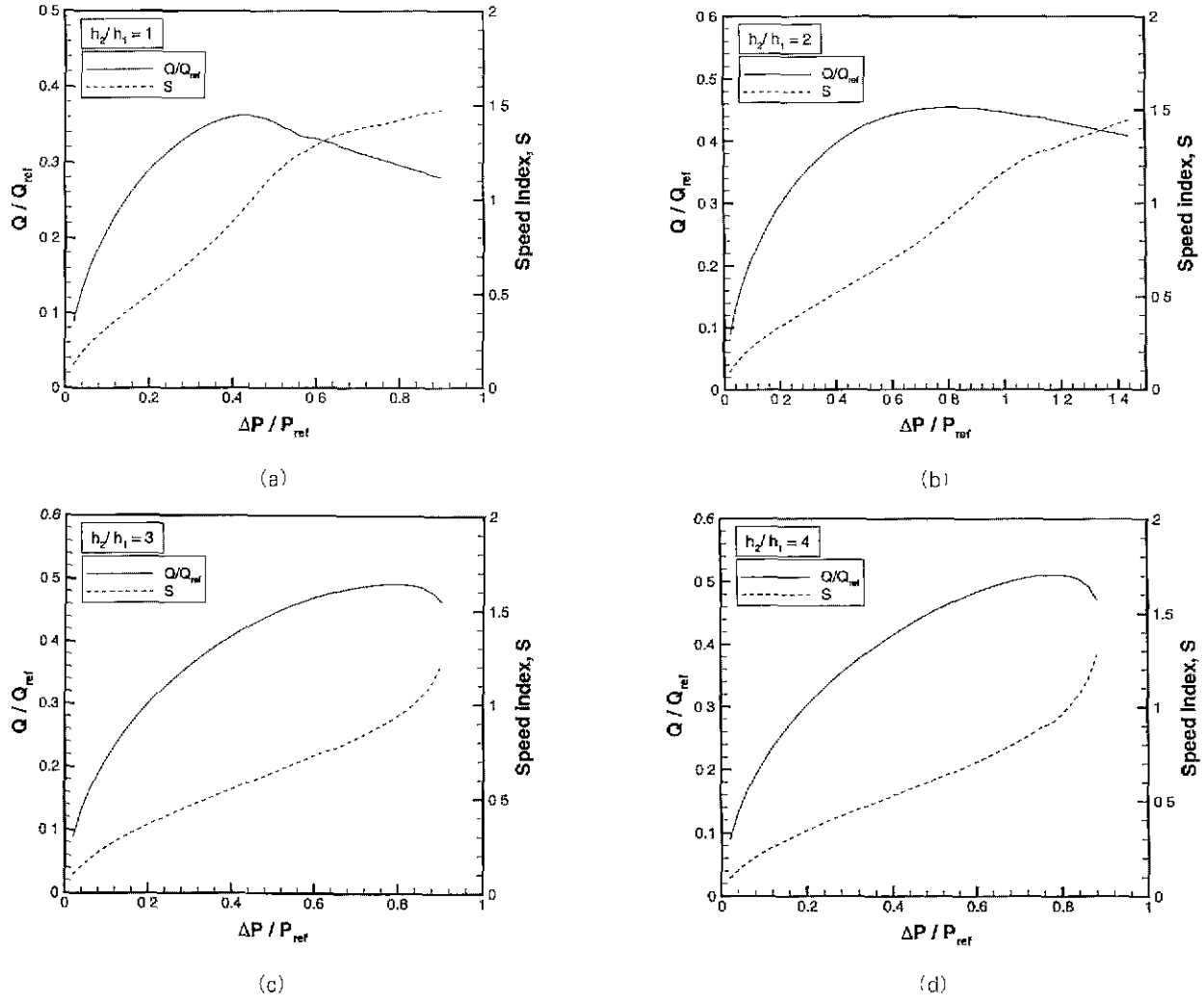

Fig. 6. Flow rate and speed index as functions of the inlet-to-outlet pressure difference for (a) $h_2/h_1=1$, (b) $h_2/h_1=2$, (c) $h_2/h_1=3$, (d) $h_2/h_1=4$

is reduced, up to the point of non-convergence (Fig. 7) Flow limitation, however, is observed (Fig. 6) and follows a pattern that is relatively uninfluenced by the degree of taper. These solutions tend to lose convergence soon after maximal flow is attained. If the pressure drop through collapsible tube exceed the condition in which the choking happens, the flow rate decreases and the tube eventually collapses due to the decreased pressure in the throat. Once the tube collapsed, the pressure in the inlet prevails to the collapsed part. Then, the increased pressure in the upstream may leads to the opening of the collapsed tube. But if the flow starts, the pressure drop along the tube cause flow limitation again This may lead to the dynamic phenomenon of waterfall effect. It is widely admitted that the flow limitation or choking are critical to analyze the waterfall effect which happens in the airways and venules of lung, vena cava, other veins[16].

The distributions of fluid pressure and solid effective stress are presented for $h_2/h_1=2$ in Fig 8. Fluid pressure decreases up to the area minimum, then increases again reflecting a degree of pressure recovery downstream of the throat. Effective stresses in the solid are large near the downstream end due to the combination of large bending effects and the highly negative transmural pressure.

In view of the tendency for flow limitation seen in these results, it is of interest to compute the speed index, S, defined as the ratio of mean fluid speed to wave speed. Here we estimate wave speed for long waves, c, using the Moens-Korteweg equation[16].

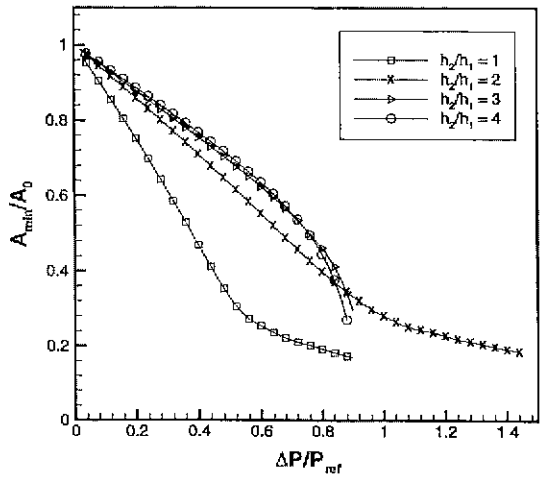

Fig. 7. Minimum cross-sectional area in the axisymmetric tube as a function of the inlet-to outlet pressure difference. Note the difference in character at high collapse for the two cases with large taper as compared to those with small taper

$$c=\left(\frac{Eh}{2\rho_f R}\right)^{1/2} \tag{9}$$

In a one-dimensional flow analysis, maximal flow occurs when S equals unity[6] This is seen to be true in the present simulations (Figure 6) when the speed index evaluated at the point of minimum cross-sectional area, based on centerline velocity, is plotted against the pressure difference. Unlike the prediction from purely one-dimensional theory, however, the flow rate is observed to decrease and S continues to rise as downstream pressure is further reduced Moreover, the profile of S vs. axial distance, z/L (Fig 9) continues to change upstream of the point where S=1, albeit slightly, following the first occurrence of critical flow. These observations could be due to the presence of longitudinal bending stiffness or tension, either of which introduce wave speed dispersion (so that waves of finite wave length travel more rapidly than predicted by eqn. (9))[17]. In fact, the possibility of a transition to supercritical flow (S>1) near the downstream attachment point had been observed experimentally and tentatively explained based on an approximate correction to the one-dimensional theory that includes these longitudinal effects[17].

With larger taper (h2/h1 = 3 and 4, Fig 6(c) & (d)), the flow rate once again reaches a maximum when S is approximately one. The fall in flow rate and the increase in speed index after the point of maximal flow, however,

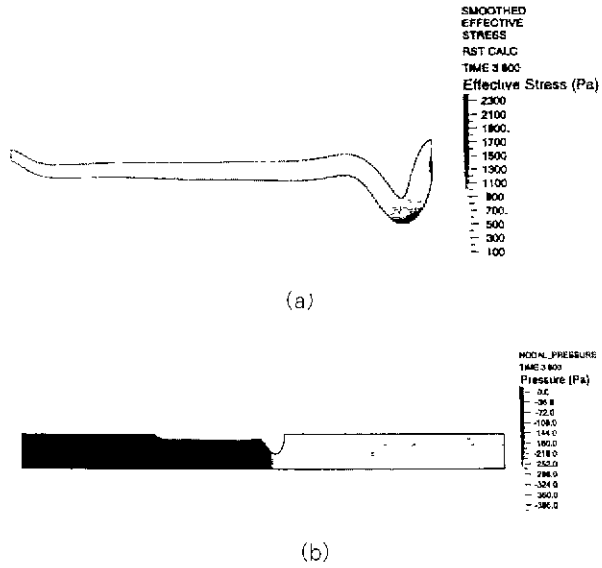

Fig. 8. Computed results for the axisymmetric tube with $h_2/h_1=2$ just prior to complete collapse (a) Distribution of effective stress in the elastic wall, (b) Distribution of pressure in the fluid domain

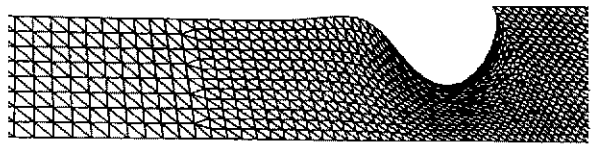

Fig. 10 Close-up of the distorted mesh in the axisymmetric tube for $h_2/h_1=1$ at $\Delta P/P_{ref}=0.6$ just prior to breakdown of the computation

are both more abrupt, and the solution fails to converge much sooner. Note that in these cases, the point of minimum area and the first occurrence of critical flow are both located near the upstream end of the tube. Downstream of this point the flow accelerates beyond S=1, then quickly decelerates to subcritical speeds, continuing to fall in the direction of increasing stiffness. While the transition to subcritical speed appears to be smooth as suggested in previous experiments and one-dimensional theory for tubes with tapered walls[18], the axisymmetric assumption of the present analysis makes it difficult to make a direct comparison.

In every case, the computations fail to converge prior to an outlet pressure of -500 Pa. This may be due to the highly distorted mesh for h_2/h_1=1 and 2 as shown in Fig. 10 In the case of h_2/h_1=3 and 4, the numerical instability appears to result from the increasingly steep reduction in minimum cross-section area as the outlet pressure decreases (Fig. 7). While the cause for lack of convergence

in these cases is unknown, it may be indicative of numerical instability, or possibly a breakdown of the steady solution leading to oscillatory behavior.

Since many of the relevant experiments were conducted on much longer tubes, we examined the effect of tube length by calculating two additional cases for the taper of h_2/h_1=1: L/R=10 and L/R=5. The flow rates and area reductions of these cases differed by no more than 4% from those of L/R=7.5, confirming that the flow phenomena in these simulations is not significantly influenced by tube length.

Conclusion

In this paper, we present the model of steady axisymmetrical flow as a step toward the analysis of fully three-dimensional and unsteady conditions. The solutions presented here agree with other published results from experiments and computational analysis, providing some degree of confidence that these same methods.

We used the full Navier-Stokes equations to describe flow within the collapsible tube, and allowed for a wall with finite thickness that undergoes large deformation These are all necessary if a realistic simulation is to be created. The true flow field occurring in collapsible tube interacting with an elastic wall has complicated characteristics certain to be influenced by viscous dissipation and possibly flow separation behind the throat of elastic wall These effects cannot be simulated with inviscid or Stokes flow assumptions. Furthermore, while most previous studies approximate the collapsible tube or channel as a membrane of zero-thickness, many of the existing experiments and real occurrences of collapsible tube flow in physiology deal with tubes that are not necessarily thin.

Numerical solutions for the collapsible tube show that flow rate reaches a maximum when the speed index is near unity at the point of minimum cross sectional area, indicative of flow limitation or choking. These consist of the main reasons of waterfall phenomenon which occurs in a number of veins. The constriction points in the tube vary according to the ratio of downstream-to-upstream wall thickness

References

1. R.D. Kamm and T J Pedley, "*Flow in Collapsible Tubes: A brief Review*", ASME Tran. J. of Biomechanical Engineering, Vol. 111, pp. 177 179, 1989
2. W A. Conrad, "*Pressure-Flow Relationalships in Collapsible Tubes*". IEEE Trans Biomedi. Engng., Vol. 16, pp. 284-295, 1969
3. R W Brower and C. Scholten, "*Experimental Evidence on the Mechanism for the Instability of Flow in Collapsible Vessels*", Med. Biol. Eng., Vol. 13, pp. 839-845, 1975
4. C.D. Bertram, 1986, Unstable Equilibrium Behavior in Collapsible Tubes, J of Biomechanics, Vol. 19, pp. 61-69, 1986
5. G C Oates, "*Fluid flow in soft-walled tubes: I. Steady flow*", Med. Biol. Eng., Vol. 13, pp. 773-778, 1975
6. A H Shapiro, "*Steady Flow in Collapsible Tubes*", ASME Trans J Biomech. Eng., Vol. 99, pp 126-147, 1977
7. C.D Bertram and T.J. Pedley, "*A Mathematical Model of Unsteady Collapsible Tube Behavior*", J. of Biomechanics, Vol 15, pp 39-50, 1982
8. T J Pedley, "*Longitudinal Tension Variation in a Collapsible Channel a New Mechanism for the Breakdown of Steady Flow*", ASME Trans. J. Biomech Eng., Vol 99, pp. 126-147, 1992
9. X.Y Luo and T J. Pedley, "*A Numerical Simulation of Steady Flow in a 2-D Collapsible Channel*", J Fluids and Struct., Vol 9, pp. 149-174, 1995
10. X.Y. Luo and T.J. Pedley, A Numerical Simulation of Unsteady Flow in a 2-D Collapsible Channel, J. Fluid Mechanics, Vol 314, pp 191-225, 1996
11. M. Heil, "*Stokes Flow in a Collapsible Tubes: Computation and Experiment*", J. Fluid Mechanics, Vol. 353, pp. 285-312, 1997
12. M. Bathe and Kamm, R D., 1998, A Fluid-Structure Interaction Finite Element Analysis of Pulsatile Blood Flow through a Compliant Stenotic Artery, ASME Tran. J. of Biomechanical Engineering, ASME J. Biomech Eng , Vol 121, pp. 361-369, 1999
13. K.J. Bathe, H Zhang and M H Wang, "*Finite Element Analysis of Incompressible and Compressible Fluid Flows with Free Surfaces and Structural Interactions*", Computers and Structures, Vol. 56, pp. 193 213, 1995
14. M Zmindak and I. Grajciar, "*Simulation of the Aquaplane Problem*", Computers and Structures, Vol. 64, pp. 1155-1164, 1997
15. N. Stergiopulos, J.E. Moore, A. Strassle, D.N. Ku and J J Meister, "*Steady Flow Tests and Demonstration of Collapse on Models of Compliant Axisym-*

metric Stenosis", Adavanced in Bioengineering BED, Vol. 26. pp 455-458. 1993

16. C G Caro, T J Pedley, R C Schroter and W.A Seed, The Mechanics of the Circulation. Oxford, Oxford University Press, 197817. M.E. McClurken, I Kececioglu, R D Kamm, A.H. Shapiro, *"Steady Supercritical Flow in Collapsible Tubes : Part 2. Theoretical Studies"*, J. Fluid Mech., Vol 114. pp. 60-67, 1981
18. D.E Jaekle, *"Critical Transitions Associated with Steady Flow in Collapsible Tubes with Varying Wall Stiffness"*, M.S. Thesis, Cambridge, MIT Press, 1987